

Electrochemical Model of Mild Steel Corrosion in a Mixed H₂S/CO₂ Aqueous Environment in the Absence of Protective Corrosion Product Layers

Yougui Zheng,* Jing Ning,* Bruce Brown,* Srdjan Nešić^{†,*}

ABSTRACT

The present study has been conducted to investigate the electrochemistry of mild steel corrosion in a mixed hydrogen sulfide/carbon dioxide (H₂S/CO₂) aqueous environment, and develop an electrochemical model to simulate the experimental results. The experiments were designed to determine the effect of H₂S on CO₂ corrosion for short-term exposures of a few hours before any interference from iron sulfide corrosion product layers happened. Tests were conducted at different H₂S concentrations, ranging from 0 to 10% in the gas phase at 1 bar total pressure at pH 4 and pH 5. Mechanisms related to H₂S/CO₂ corrosion have been examined by using different techniques such as linear polarization resistance (LPR) using the scan rate 0.125 mV/s, potentiodynamic sweeps (scan rate 1 mV/s), and comparison of experimental results with electrochemical model predictions. Results indicate that the presence of H₂S could affect both cathodic reactions and the anodic reaction. An electrochemical model was developed for a mixed H₂S/CO₂ system, which was calibrated with new experimental results and compared to data found in the open literature. The model predictions fit experimental data well for short exposures (measured in hours) but overestimate the experimental results for longer term exposures (measured by days and weeks) due to the formation of an iron sulfide corrosion product layer, which is not accounted for in the present model.

KEY WORDS: carbon dioxide, carbon steel, corrosion rate, hydrogen sulfide, modeling, uniform corrosion

Submitted for publication: March 18, 2014. Revised and accepted: September 10, 2014. Preprint available online: September 22, 2014, <http://dx.doi.org/10.5006/1287>.

[†] Corresponding author. E-mail: nesic@ohio.edu.

* Institute for Corrosion and Multiphase Technology, Department of Chemical and Biomolecular Engineering, Ohio University, 342 W. State St., Athens, OH 45701.

INTRODUCTION

Corrosion in a mixed carbon dioxide/hydrogen sulfide (CO₂/H₂S) aqueous environment is an important issue in the oil and gas industry. More attention has been focused on this type of corrosion because of harsher environments encountered when exploring new sources of oil and gas, which often contain H₂S. However, little progress has been made in defining the corrosion mechanisms involved. The understanding, prediction, and control of H₂S corrosion are some of the key challenges for oil and gas production.

The severity of corrosion depends on multiple factors, including temperature, pH, partial pressures of CO₂ and H₂S, and flow conditions, to name the most important ones. Therefore, there is a need for models that can predict corrosion rates under various conditions and, thus, save the cost of performing numerous experiments.

Models for CO₂ corrosion have been developed in the past, taking the form of semi-empirical correlations or mechanistic models describing the different processes involved in CO₂ corrosion of carbon steel.¹⁻² In the case of H₂S corrosion, there are numerous experimental studies;³⁻⁸ however, only a few models have been developed and published in the open literature for H₂S or mixed CO₂/H₂S corrosion.⁹⁻¹⁰

Anderko and Young⁹ presented a mechanistic model to simulate the corrosion rates of carbon steel in a mixed CO₂/H₂S environment. The model consists of a thermodynamic part used to predict corrosion-product layer composition and an electrochemical

model to simulate the rate of cathodic and anodic processes on the metal surface. However, the electrochemical model was simplistically correlated to final steady-state corrosion rate data to obtain a good agreement by using a surface coverage effect by iron sulfide. No mechanistic verification of this approach was done with electrochemical kinetic data, and the steel-surface water chemistry was not distinguished from bulk water chemistry in their model.

Sun and Nešić¹⁰ published a mechanistic model based on a mass-transfer control mechanism for corrosion in the presence of iron sulfide layers, often seen in H₂S corrosion. This mechanistic model was calibrated to fit a broad range of experimental results and was found to be useful for the prediction of transient corrosion rates arising from the growth of iron sulfide layers. The model includes a number of assumptions that were not explicitly verified, however. For example, it was universally assumed in the model that mass transfer limits the rate of H₂S corrosion and, therefore, the electrochemical processes were not defined or included. This is clearly a simplification and limitation of the model that needed improvement.

In the first author's previous research,¹¹ an electrochemical model of carbon steel corrosion in a pure H₂S system was described and verified with electrochemical kinetics experiments. The model accounts for the effect of P_{H₂S}, flow rate, pH, and temperature on H₂S corrosion. An additional cathodic reaction, direct H₂S reduction, was identified and included in the model. In reality, CO₂ is ubiquitous, however, so it is of key importance to extend this electrochemical model to cover mixed H₂S/CO₂ systems and include validation by more literature data. The results of this work are presented.

EXPERIMENTAL

Equipment

Experiments were performed at atmospheric pressure in a 2-L glass cell with 1 wt% sodium chloride (NaCl) in deionized water solution. An experimental set-up similar to that of Zheng, et al.,¹¹ was used. A mixture of H₂S and CO₂ gas was sparged through the cell continuously. A typical three-electrode setup was used. The working electrode (WE) was a rotating cylinder electrode (RCE) made of mild steel with a speed controller. The counter electrode (CE) was a concentric ring made of platinum wire. The reference electrode (RE) was a saturated silver-silver chloride (Ag/AgCl) electrode connected to the cell externally via a Luggin capillary. The pH was monitored with an electrode immersed in the electrolyte. The concentration of H₂S was adjusted by a gas rotameter and measured by a gas sample pump with H₂S detector tubes. A carbon scrubber was used to treat the gas coming out of glass cell to remove the H₂S.

Materials

API 5L-X65 pipeline steel was used in the present experiments with a composition (as reported by the manufacturer) shown in Table 1. The WE was machined out from the parent steel material and had a diameter of 1.20 cm and a working surface area of 5.4 cm².

Procedure

The aqueous solution was initially deoxygenated by continuously purging CO₂ gas for at least 3 h. At the same time, the solution was heated to the desired temperature. After the solution was deoxygenated, H₂S was added to the purge for at least 30 min to saturate the solution at the required partial pressure of H₂S. The pH was adjusted by adding deoxygenated hydrochloric acid (HCl) or sodium hydroxide (NaOH). Prior to immersion, the cylindrical X65 mild steel specimen surfaces were polished sequentially with 400 and 600 grit sandpaper, while being cooled simultaneously with isopropyl alcohol, then were washed with isopropyl propanol in an ultrasonic cleaner and dried with an air blower.

The gas concentration was adjusted by purging different H₂S/CO₂ ratios, from 100 ppm H₂S (P_{H₂S} = 0.1 mbar) to 10% H₂S (P_{H₂S} = 96.5 mbar) in the mixed H₂S/CO₂ gas at 30°C. Table 2 shows the unit conversion of ppm or % to mbar for H₂S concentration in gas phase. The unit of ppm or % used here is based on a volume fraction (volume H₂S in the total mixture of H₂S/CO₂ gas). Only the dry gas mixture of H₂S and CO₂ without water vapor was measured before purging into the glass cell system. There is always some water vapor in the gas phase of any system containing water. When converting ppm or % to partial pressure of H₂S, the water vapor pressure must be considered, especially in high temperature environments.

A potentiostat was used to perform electrochemical measurements during the test. The open circuit potential (OCP) was monitored and polarization resistance (R_p) measurements were conducted by polarizing the WE ±5 mV from the free corrosion potential and scanning at 0.125 mV/s. Solution resistance was measured independently using electrochemical impedance spectroscopy (EIS), and the measured R_p was then corrected. The corrosion rate (CR) was calculated based on measured R_p by using the LPR constant B = 23 mV/decade. EIS measurements were carried out by applying an oscillating potential ±5 mV around OCP of the WE, using the frequency range 3 mHz to 5 kHz. At the end of each experiment, the potentiodynamic sweeps

TABLE 1

Chemical Composition of 5LX65 used in RCE (wt%)

Cr	Mo	S	V	Si	C	Fe	Ni	Mn	P
0.14	0.16	0.009	0.047	0.26	0.13	Bal.	0.36	1.16	0.009

TABLE 2

The Unit Conversion of ppm or % to mbar for H₂S in Gas Phase at 30°C, 1 Bar Total Pressure

H ₂ S volume fraction in the total mixture H ₂ S/CO ₂ gas	100 ppm	500 ppm	0.65%	6%	10%
H ₂ S partial pressure/mbar	0.1	0.5	6.3	58.2	96.5

were conducted at a scan rate of 1 mV/s. The cathodic sweep was performed first by beginning at the OCP; the electrode was then allowed to equilibrate back to the OCP; and finally, the anodic sweep, starting at the OCP, was conducted. The solution resistance was manually corrected for after the measurements.

The test matrix for the experimental work is shown in Table 3. The duration of the experiments was intentionally short, and the pH and temperature were low, in order to avoid formation of protective corrosion product layers (such as sulfides, carbonates, and oxides), which complicate the corrosion process and make interpretation of electrochemical measurements very difficult.⁽¹⁾

RESULTS AND DISCUSSION

Effect of P_{H_2S}

Corrosion rates at different H₂S concentrations in the H₂S/CO₂ mixture, pH 4, and 1,000 rpm rotating speed condition are shown in Figure 1. The corrosion rate under a pure CO₂ environment (zero H₂S concentration) at pH 4 was about 2.7 mm/year. When H₂S gas concentration was increased to 100 ppm and 500 ppm, the corrosion rates decreased to 1.4 mm/year and 1.5 mm/year and then increased again to 2.4 mm/year at 10% H₂S gas concentration. A similar corrosion behavior was observed at pH 5 (Figure 2). This trend has been also observed by the authors in a pure H₂S environment¹¹ and other researchers^{6,12-15} in a mixed H₂S/CO₂ environment. The change of corrosion rate is due to the effect of H₂S on both cathodic reactions and the anodic reaction, which is shown in Figure 3 and Figure 4 and explained in the following text.

The effect of H₂S on cathodic potentiodynamic sweeps at pH 4 and pH 5 are shown in Figure 3 and Figure 4. At pH 4, the cathodic potentiodynamic sweep in a pure CO₂ aqueous environment (without any H₂S) has the same shape that has previously been reported by others.¹⁶ It shows a limiting cathodic current region in the range of -720 mV to -900 mV, which consists of the diffusion-limited current of H⁺ reduction and the chemical-reaction-controlled current of carbonic acid (H₂CO₃) reduction. At a more negative potential, a charge-transfer current region is seen corresponding to direct water (H₂O) reduction. When 100 ppm or 500 ppm H₂S was introduced, the

TABLE 3

Test Matrix

Description	Parameters
Test material	API 5L X-65
Test solution	1 wt% NaCl solution
Purge gas (H ₂ S volume fraction in H ₂ S/CO ₂)	0-10%(v) (0-0.1 bar)
Rotating speed /rpm	1,000
Total pressure/bar	1
Temperature/°C	30
pH	4, 5
Test duration/hour	0.5 to 2
Measurement methods	LPR, EIS, potentiodynamic sweeps

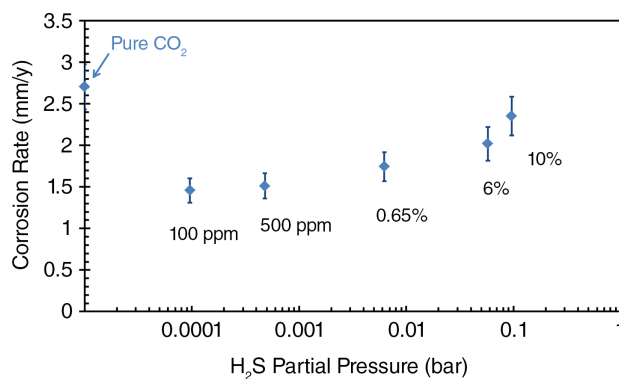


FIGURE 1. Effect of H₂S gas concentration in the H₂S/CO₂ mixture at total pressure 1 bar, on corrosion rates of X65 mild steel at pH 4, 30°C, 1 wt% NaCl, 1,000 rpm rotating speed, exposure time < 2 h, B = 23 mV/decade.

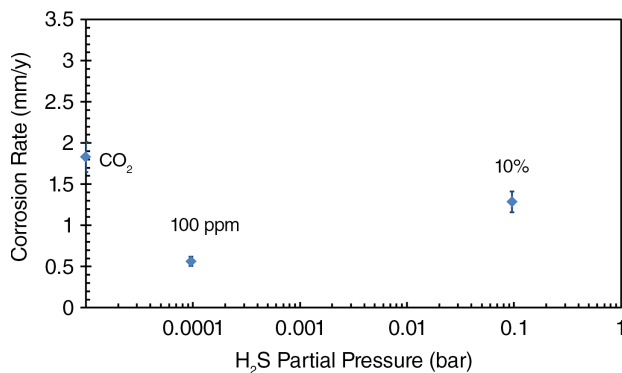


FIGURE 2. Effect of H₂S gas concentration in the H₂S/CO₂ mixture at total pressure of 1 bar, on corrosion rates of X65 mild steel at pH 5, 30°C, 1 wt% NaCl, 1,000 rpm rotating speed, exposure time < 2 h, B = 23 mV/decade.

⁽¹⁾ The sample surface examined with EDS and XRD. EDS after the exposure showed a small peak of sulfur, but XRD results indicated that no iron sulfide crystals formed on the steel surface.

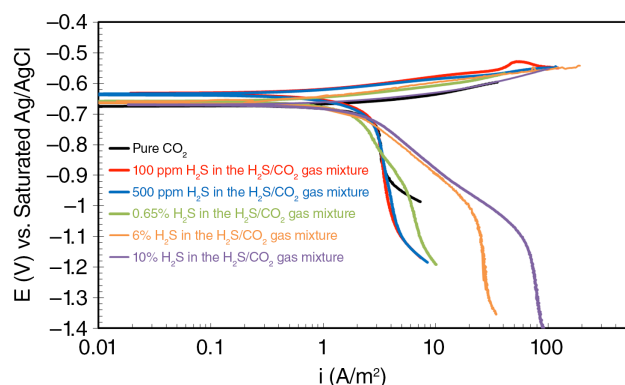


FIGURE 3. Effect of H_2S gas concentration in the H_2S/CO_2 mixture at total pressure 1 bar on potentiodynamic sweeps of X65 mild steel corrosion at pH 4, 30°C, 1 wt% NaCl, 1,000 rpm rotating speed, exposure time < 2 h.

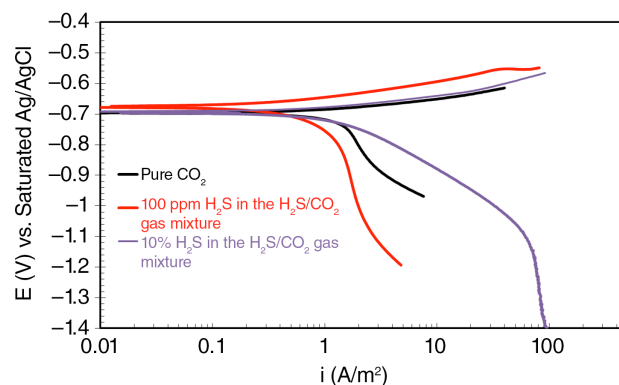
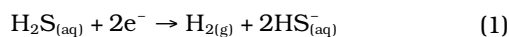


FIGURE 4. Effect of H_2S gas concentration in the H_2S/CO_2 mixture at total pressure 1 bar on potentiodynamic sweeps of X65 mild steel corrosion at pH 5, 30°C, 1 wt% NaCl, 1,000 rpm rotating speed, exposure time < 2 h.

mass-transfer limiting current did not change, compared with a pure CO_2 purged environment, and the H_2O reduction rate was slowed down; this agreed with the observation reported previously for a pure H_2S environment (without CO_2)¹¹ and a mixed H_2S/CO_2 environment.⁷ As the H_2S gas concentration increased (to 0.65% and higher to 10%), the cathodic limiting current plateau moved to higher currents and a second “wave” in the limiting current at more cathodic potential also appeared, which is due to the direct reduction of H_2S on the steel surface according to:¹¹

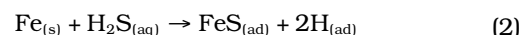


At pH 5, the same trend in the cathodic potentiodynamic sweep with H_2S concentration was observed. The mass-transfer limiting current did not change at 100 ppm H_2S , but increased at 10% H_2S . The retardation effect of H_2S on the H_2O reduction rate was also observed.

The decrease in the rate of H_2O reduction due to H_2S was clearly observed at both pH 4 and pH 5. However, the effect of H_2S on the charge transfer kinetics of H_2CO_3 reduction was not as clear from the potentiodynamic sweeps because of the interference by the anodic iron (Fe) dissolution reaction and the limiting current control of the cathodic reaction. Both H_2O reduction and H_2CO_3 reduction are different pathways for the hydrogen evolution reaction, however; therefore, it is reasonable to postulate that the same retardation effect seen for H_2O reduction holds true for the H_2CO_3 reduction reaction as well. This assumption was confirmed through comparisons between experimental results and model predictions, as described below.

This retardation effect due to H_2S has been previously proposed to be due to the very rapid formation of a thin mackinawite film, formed by direct reaction of H_2S with Fe, via a so-called “solid state reaction.”

The mechanism of this thin mackinawite film formation was first proposed by Shoesmith, et al.,¹⁷ and used in Sun and Nešić’s mechanistic model.¹⁰ An alternative mechanism is adopted here. A very thin iron sulfide film forms very rapidly via a chemisorption process, i.e., by a direct reaction of exposed surfaces of Fe with H_2S , as suggested by Marcus, et al.¹⁸ The mechanism is also supported in the work of Smith and Wright.¹⁹



This adsorbed sulfide film can displace adsorbed H_2O and OH^- as indicated by Marcus, et al.,¹⁸ and probably affect the double layer composition. Therefore the kinetics of electrochemical reactions is slowed down. This retardation effect has also been observed for platinum electrodes²⁰ and iridium electrodes,²¹ where the hydrogen evolution rate was significantly retarded.

The effect of H_2S concentration on the anodic Fe dissolution reaction at pH 4 and pH 5 can also be seen in the potentiodynamic sweeps (Figure 3 and Figure 4). At pH 4 (Figure 3), with 100 ppm and 500 ppm H_2S gas concentration, the anodic potentiodynamic sweeps shifted to the lower current direction, as compared with a pure CO_2 environment. This indicates a retardation effect of low H_2S concentration on Fe dissolution rate, which means that the anodic reaction rate is slowed down at low H_2S concentrations. As H_2S gas concentration increased up to 6% and 10% in the H_2S/CO_2 gas mixture, the anodic reaction rate increased, and eventually reached the same rate as in a pure CO_2 environment. At pH 5 (Figure 4), the similar behavior of the anodic potentiodynamic sweeps was observed, which agrees with the results previously reported in a pure H_2S environment.¹¹ This is related to HS^- adsorption on the steel surface.

According to the finding of Bockris, et al.,²² in the strong acid solution, the Fe dissolution rate is attrib-

uted to OH^- adsorption on the Fe surface. When H_2S is present, HS^- can be strongly chemisorbed on the $\text{Fe}^{20,23}$ to displace adsorbed OH^- and slow down the Fe dissolution rate at low HS^- concentration. However, analogous to the OH^- mechanism of Fe dissolution, HS^- can also accelerate this process with the increase of H_2S gas concentration.

In summary, the presence of H_2S in a CO_2 dominated aqueous environment affects both the cathodic and anodic reactions, and may lead to either acceleration or retardation of the corrosion rate of the steel, depending on H_2S concentration. For the cathodic reactions, a new cathodic reaction, direct reduction of H_2S , is confirmed.¹¹ The H_2O reduction rate is slowed down in the presence of the H_2S . The charge-transfer kinetics of H_2CO_3 reduction is also postulated to be slowed down, as well. For the anodic reaction, the same phenomena were observed as seen in pure H_2S environments,¹¹ which are dependent primarily on HS^- concentration.

Effect of pH

Solution Without H_2S — The effect of pH in an aqueous solution saturated with CO_2 (without any H_2S) on potentiodynamic sweeps is shown in Figure 5. The change of pH from pH 4 to pH 5 agrees with the previous findings of Nešić et al.¹⁶ The limiting current density decreased by a factor 2 to 3, and not 10, because of the contribution from a chemical reaction-limited H_2CO_3 reduction. Figure 5 also shows that pH had a very small effect on the anodic reaction from pH 4 to pH 5.

Solution with H_2S — The change of the potentiodynamic sweeps from pH 4 to pH 5 in an aqueous solution purged with 100 ppm H_2S in the gas mixture (Figure 6) has the same trend as that in a pure CO_2 purged solution, for both cathodic and anodic parts.

When H_2S concentration increased to 10%, the effect of pH on potentiodynamic sweeps is shown in Figure 7. The limiting current was almost the same at pH 4 and pH 5, which is different behavior from a three-fold change in pH seen in a “ CO_2 only” environment. The reason is that the main contribution to the cathodic-limiting current at 10% H_2S concentration is from the aqueous H_2S species, the concentration of which is independent of pH.

Both Figure 6 and Figure 7 show that pH had a smaller effect on the anodic dissolution reaction in the range of conditions studied.

ELECTROCHEMICAL MODEL

Anodic Reaction

The only anodic reaction is Fe dissolution from the steel surface:

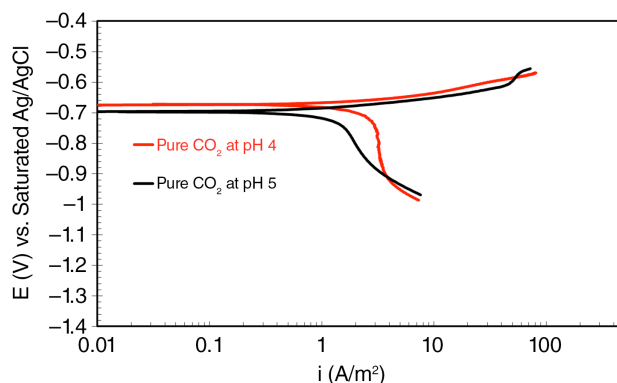


FIGURE 5. Effect of pH on potentiodynamic sweeps of X65 mild steel corrosion in the solution purged with pure CO_2 at 30°C, total pressure of 1 bar, 1 wt% NaCl, 1,000 rpm rotating speed, exposure time < 2 h.

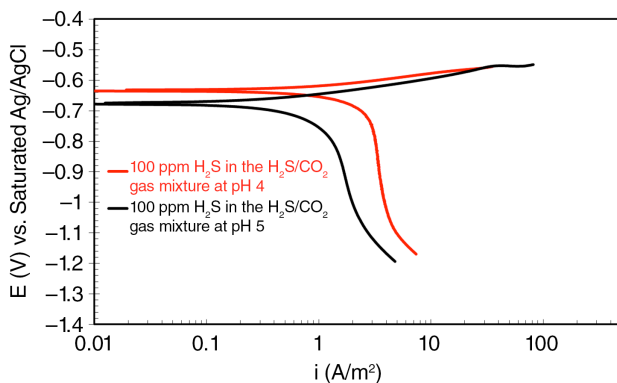


FIGURE 6. Effect of pH on potentiodynamic sweeps of X65 mild steel corrosion in the solution purged with 100 ppm H_2S in the $\text{H}_2\text{S}/\text{CO}_2$ gas mixture at total pressure of 1 bar, 30°C, 1 wt% NaCl, 1,000 rpm rotating speed, exposure time < 2 h.

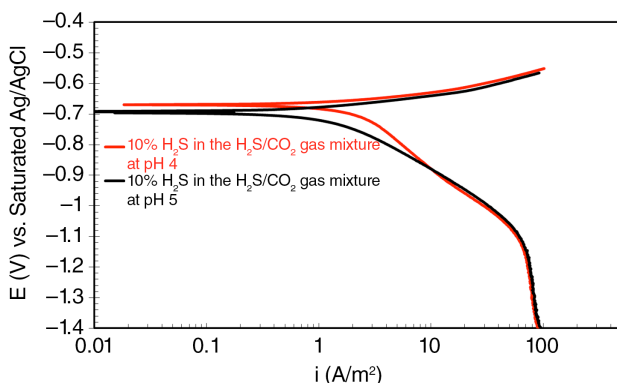


FIGURE 7. Effect of pH on potentiodynamic sweeps of X65 mild steel corrosion in the solution purged with 10% H_2S in the $\text{H}_2\text{S}/\text{CO}_2$ gas mixture at total pressure of 1 bar, 30°C, 1 wt% NaCl, 1,000 rpm rotating speed, exposure time < 2 h.

A detailed model of Fe dissolution in a CO₂ environment without H₂S has been reported by Nešić et al.¹⁶ This reaction is under charge-transfer control. Thus, pure Tafel behavior can be assumed close to the corrosion potential.

$$i_{\text{Fe}} = i_{0,\text{Fe}} \times 10^{\frac{\eta}{b_a}} \quad (4)$$

The reference exchange current density $i_{0,\text{Fe}}^*$ at room temperature, 293.15K, is 1 A/m² for X-65 steel. The activation energy ΔH was found to be 37.5 kJ/mol. The Tafel slope is $b_a = \frac{2.303RT}{1.5F}$. The reversible potential of X-65 steel was taken to be -0.488 V.¹⁶

When H₂S is present, the anodic reaction rate is observed to mostly depend on H₂S concentration, as shown in Figures 3 and 4. This behavior is modeled as proposed in the previous study,¹¹ where the exchange current density is related to the surface coverage by HS⁻ ions (θ_{HS^-}) and follows the Langmuir adsorption model, as shown in Equations (5) and (6). K_2 is the Langmuir adsorption constant, which is obtained from the previous study.¹¹

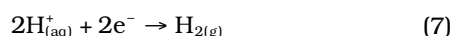
$$i_{0,\text{Fe}} = i_{0,\text{Fe}}^* \theta_{\text{HS}^-} e^{\frac{\Delta H}{R} \left(\frac{1}{T} - \frac{1}{T_{\text{ref}}} \right)} \quad (5)$$

$$\theta_{\text{HS}^-} = \frac{K_2 C_{\text{HS}^-}}{1 + K_2 C_{\text{HS}^-}} \quad (6)$$

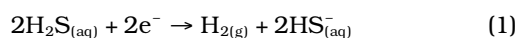
Cathodic Reactions

In the model, there are four cathodic reactions in a mixed CO₂/H₂S aqueous system:

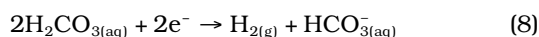
—reduction of H⁺ ions:



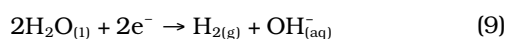
—direct reduction of aqueous H₂S (as described in the previous study):¹¹



—direct H₂CO₃ reduction:



—direct H₂O reduction:



The details of H⁺ reduction, H₂S reduction, and H₂O reduction have been described in a previous paper,¹¹ which covers these same reactions for a pure H₂S system, and no change is made in the present work for a mixed CO₂/H₂S aqueous system. The modeling of H₂CO₃ reduction with and without H₂S is done differently, however, and will be addressed below.

Modeling of H₂CO₃ reduction for a pure CO₂ aqueous system (without H₂S) has been described clearly by Nešić et al.¹⁶ The total current density of H₂CO₃ reduction is given by:

$$\frac{1}{i_{\text{H}_2\text{CO}_3}} = \frac{1}{i_{\alpha,\text{H}_2\text{CO}_3}} + \frac{1}{i_{\text{lim},\text{H}_2\text{CO}_3}^f} \quad (10)$$

where $i_{\text{H}_2\text{CO}_3}$, $i_{\alpha,\text{H}_2\text{CO}_3}$, and $i_{\text{lim},\text{H}_2\text{CO}_3}^f$ are the total current density, the charge transfer current density, and the mass transfer limiting current density of this reaction in A/m², respectively.

Charge transfer current density of this reaction can be calculated using the equation:

$$i_{\alpha,\text{H}_2\text{CO}_3} = i_{0,\text{H}_2\text{CO}_3} \times 10^{\frac{\eta}{b_c}} \quad (11)$$

Tafel slope and reversible potential can be calculated from Equation (12) and (13):

$$b_c = \frac{2.303RT}{\alpha_c F} \quad (12)$$

$$E_{\text{rev}} = -\frac{2.303RT}{F} \text{pH} - \frac{2.303RT}{2F} \log P_{\text{H}_2} \quad (13)$$

$\alpha_c = 0.5$, giving $b_c \approx 0.120$ V/decade at 30°C, and the P_{H_2} set to 1 bar.

The exchange current density can be calculated by:

$$i_{0,\text{H}_2\text{CO}_3} = i_0^{\text{ref}} \left(\frac{C_{\text{H}_2\text{CO}_3}}{C_{\text{H}_2\text{CO}_3}^{\text{ref}}} \right)^{0.5} \left(\frac{C_{\text{H}^+}}{C_{\text{H}^+}^{\text{ref}}} \right)^{-0.5} \times e^{\frac{\Delta H}{R} \left(\frac{1}{T} - \frac{1}{T_{\text{ref}}} \right)} \quad (14)$$

From Nešić,^{16,24} the $i_{0,\text{ref}}$ for H₂CO₃ reduction was taken to be 0.018 A/m² at 293.15K reference temperature and 1×10⁻⁴ mol/L reference H₂CO₃ concentration. The enthalpy of activation in Equation (5) is set to 50 kJ/mol.¹⁶

The CO₂ hydration reaction limiting current density can be calculated using:¹⁶

$$i_{\text{lim}(\text{H}_2\text{CO}_3)}^f = f \times F \times c_{\text{CO}_2} \times (D_{\text{H}_2\text{CO}_3} K_{\text{hyd}} k_{\text{hyd}}^f)^{0.5} \quad (15)$$

where c_{CO_2} is the bulk concentration of dissolved carbon dioxide, which can be obtained from:

$$c_{\text{CO}_2} = K_{\text{sol}} * P_{\text{CO}_2} \quad (16)$$

Henry's constant K_{sol} as a function of temperature can be calculated using:²⁴

$$K_{\text{sol}} = \frac{14.5}{1.00258} \times 10^{-(2.27+5.65^{-3}T_f - 8.06 \times 10^{-6}T_f^2 + 0.075I)} \quad (17)$$

where T_f is temperature in degrees Fahrenheit and $I = \frac{1}{2} \sum_i c_i z_i^2$ is ionic strength in molar.

The equilibrium constant for the CO₂ hydration reaction, K_{hyd} , is equal to 2.58×10^{-3} and does not change with temperature.²⁴ The forward hydration reaction constant (k_{hyd}^f) is a function of temperature, which is given as:²⁵

$$k_{\text{hyd}}^f = 10^{329.85 - 110.541 \times \log T_k - \frac{17265.4}{T_k}} \quad (18)$$

where T_k is absolute temperature in Kelvin.

From experimental observation, it was found that when H₂S was present, the H₂O reduction rate was slowed down by approximately 1 or 2 orders of magnitude. Similarly, it is considered here that H₂CO₃ reduction was also slowed down, due to the presence of H₂S. Here, a factor of 3 was chosen, based on comparison between experimental results and model predictions. This factor can probably change with H₂S concentration or other parameters, and needs further investigation. Therefore, the i_0^{eff} for H₂CO₃ reduction was taken to be 0.006 A/m², 3 times lower than the 0.018 A/m² used for a pure CO₂ environment without H₂S. The other parameters were taken to be the same as in the model without H₂S.

The Mixed Potential Theory

The model requires, as input, temperature, pH, $P_{\text{H}_2\text{S}}$, P_{CO_2} , and the hydrodynamic parameters, in this case, the rotating cylinder diameter, and the rotational velocity. The corrosion potential then can be calculated by solving the charge balance equation:

$$\sum i_a = \sum i_c \quad (19)$$

which here takes the form:

$$i_{\text{Fe}} = i_{\text{H}_2\text{CO}_3} + i_{\text{H}_2\text{S}} + i_{\text{H}^+} + i_{\text{H}_2\text{O}} \quad (20)$$

Once the corrosion potential is found, the corrosion current and rate can be found from the anodic current (or total cathodic current) at the corrosion potential. The individual and total cathodic and anodic curves and predicted potentiodynamic sweeps can be generated.

MODEL VALIDATION

Performance of the model was validated by comparing the calculations with the experimental results described above and with the external data obtained from the open literature.

Comparison with Results from the Present Experimental Study

First, the electrochemical model in a pure CO₂ environment without H₂S is validated with the experimental results at pH 4 and pH 5. Figure 8 and Figure 9 show the comparison of the potentiodynamic

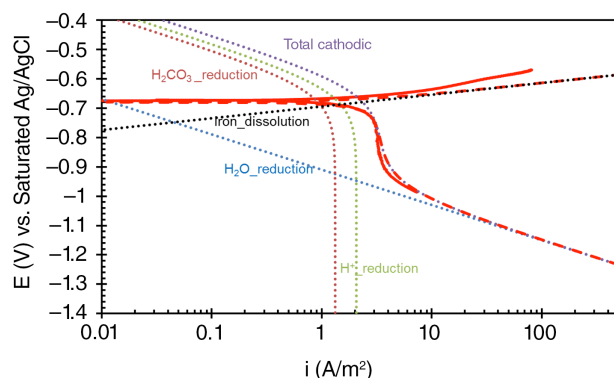


FIGURE 8. Comparison between predicted potentiodynamic sweeps and experimental results in the solution purged with pure CO₂ at pH 4, 30°C, total pressure of 1 bar, 1 wt% NaCl, 1,000 rpm rotating speed, exposure time < 2 h. Solid line: experimental sweeps. Dashed line: predicted sweeps.

sweeps simulated by the model with experimental data. It can be seen that the potentiodynamic sweeps capture the corrosion processes very well and the calculated results are in a very good agreement with all experimental results.

Second, the effect of H₂S addition was simulated with the electrochemical model. Figure 10 and Figure 11 show the comparisons of simulated sweeps with experimental results at pH 4 and at pH 5. Model simulations capture cathodic and anodic potentiodynamic sweeps changes with increasing H₂S gas concentration, and generally agree with experimental potentiodynamic sweeps at different H₂S concentrations. Figure 12 and Figure 13 show that the corrosion rates calculated by the electrochemical model are in good agreement with experimental results, all of which suggests that the electrochemical model captures the main electrochemical processes underlying H₂S/

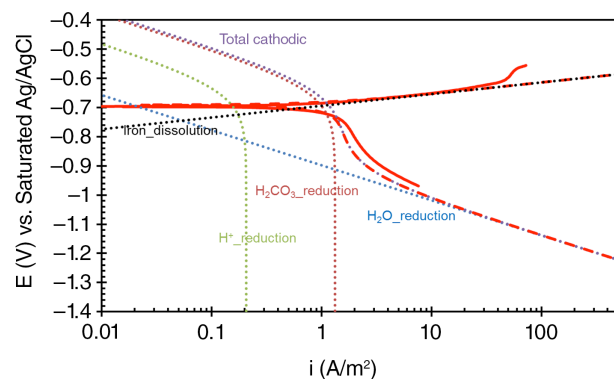


FIGURE 9. Comparison between predicted potentiodynamic sweeps and experimental results in the solution purged with pure CO₂ at pH 5, 30°C, total pressure of 1 bar, 1 wt% NaCl, 1,000 rpm rotating speed, exposure time < 2 h. Solid line: experimental sweeps. Dashed line: predicted sweeps.

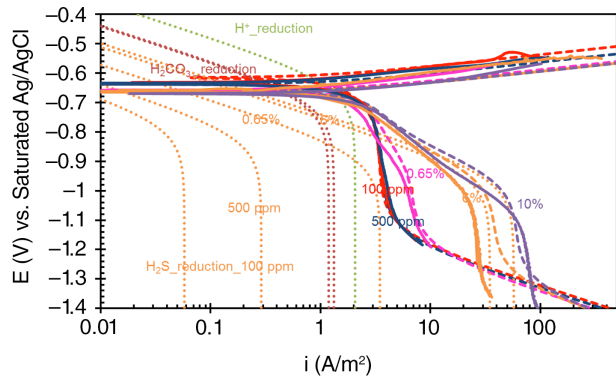


FIGURE 10. Comparison of predicted potentiodynamic sweeps with experimental results in the solution purged with different H_2S gas concentrations in the H_2S/CO_2 gas mixture at pH 4, 30°C, total pressure of 1 bar, 1 wt% NaCl, 1,000 rpm rotating speed, exposure time < 2 h. Solid line: experimental sweeps. Dashed line: predicted sweeps. Red: 100 ppm H_2S/CO_2 , Dark blue: 500 ppm H_2S , Pink: 0.65% H_2S , Orange: 6% H_2S , Purple: 10% H_2S in the H_2S/CO_2 gas mixture.

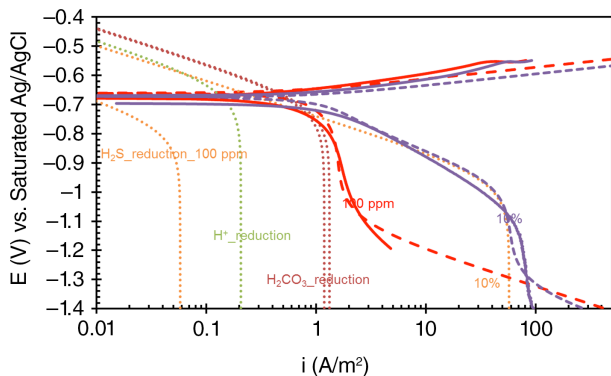


FIGURE 11. Comparison of predicted potentiodynamic sweeps with experimental results in the solution purged with different H_2S gas concentrations in the H_2S/CO_2 gas mixture at pH 5, 30°C, total pressure of 1 bar, 1 wt% NaCl, 1,000 rpm rotating speed, exposure time < 2 h. Solid line: experimental sweeps. Dashed line: predicted sweeps. Red: 100 ppm H_2S , Purple: 10% H_2S in the H_2S/CO_2 gas mixture.

CO_2 corrosion. Moreover, four main individual electrochemical reactions (H^+ reduction, H_2CO_3 reduction, H_2S reduction, and Fe dissolution) changing with H_2S concentration can be seen clearly in Figure 10 and Figure 11. At low H_2S gas concentrations (100 ppm or 500 ppm), the corrosion rate is lower, as compared to the pure CO_2 system (almost half, Figure 12), because both the cathodic and anodic reactions (such as Fe dissolution, H_2CO_3 reduction, and H_2O reduction) are retarded with the presence of H_2S . With the increase of H_2S concentration, the corrosion rate increases because the cathodic reactions are accelerated with the increase of H_2S reduction rate, and the anodic reaction is accelerated with HS^- concentration.

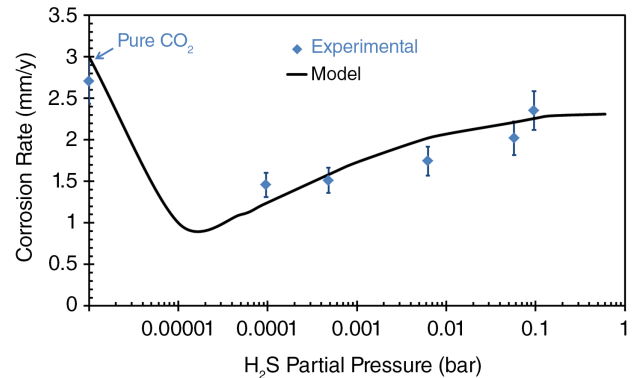


FIGURE 12. Comparison of corrosion rate predictions with experimental results in the solution purged with different H_2S gas concentrations in the H_2S/CO_2 gas mixture at pH 4, 30°C, total pressure of 1 bar, 1 wt% NaCl, 1,000 rpm rotating speed, exposure time < 2 h.

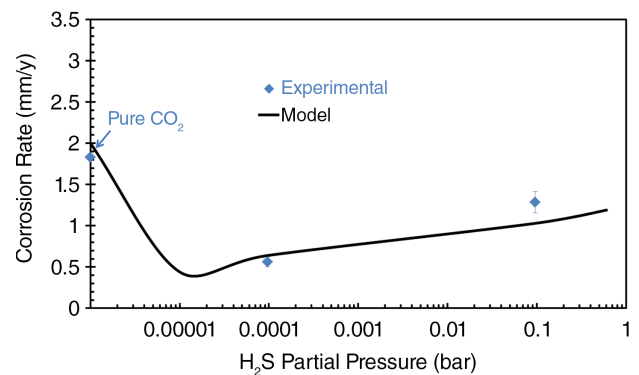


FIGURE 13. Comparison of corrosion rate predictions with experimental results in the solution purged with different H_2S gas concentrations in the H_2S/CO_2 gas mixture at pH 5, 30°C, total pressure of 1 bar, 1 wt% NaCl, 1,000 rpm rotating speed, exposure time < 2 h.

Comparison with Results of External Experimental Studies

The electrochemical model was also validated with external data obtained from the open literature. Model performance was examined first in low partial pressure of H_2S (P_{H_2S} ranged from 0.05 mbar to 0.33 mbar, corresponding to 55 ppm to 340 ppm in the gas phase at 1 bar CO_2), where the experiments were conducted by Lee.²⁶ Figure 14 shows that the corrosion rates change with H_2S partial pressure. It shows that even a very low concentration of H_2S (50 ppm or 0.05 mbar) can reduce a CO_2 corrosion rate that is greater than 1 mm/y in the absence of H_2S . The model captures this effect clearly.

Corrosion experiments at a somewhat higher concentration of H_2S (P_{H_2S} ranging from 1 mbar to 9.8 mbar, corresponding to 1,000 ppm to 10,000 ppm H_2S in the mixed H_2S/CO_2 gas phase) were reported by Choi.¹³ Model predictions are compared with the

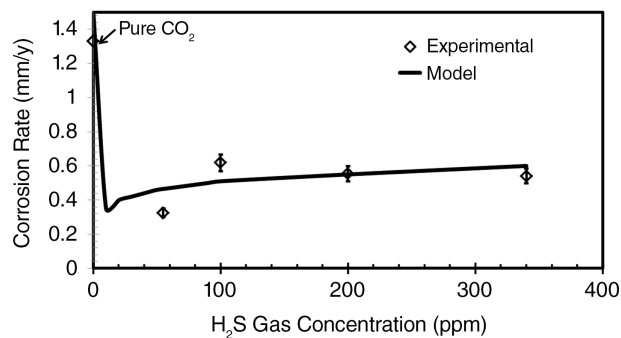


FIGURE 14. Comparison of corrosion rate predictions with experimental results in the solution purged with different partial pressures of H_2S gas in the H_2S/CO_2 gas mixture at total pressure of 1.0 bar, at pH 5, 20°C, 1 wt% NaCl, 1,000 rpm, exposure time < 1 h. Data taken from Lee.²⁶

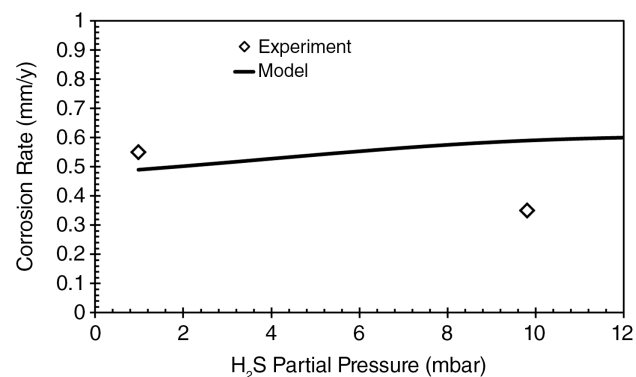


FIGURE 15. Comparison of corrosion rate predictions with experimental results in the solution purged with different partial pressures of H_2S gas in the H_2S/CO_2 gas mixture at total pressure of 1.0 bar, at pH 4, 25°C, 1 wt% NaCl, stagnant solution (0.01 m/s used in model), exposure time < 1 h. Data taken from Choi, et al.¹³

experimental results in Figure 15. Corrosion rates do not change much with H_2S concentration from 1 mbar to 9.8 mbar, which is broadly captured by the model.

The effect of temperature on corrosion rate was investigated by Abayarathna, et al.,²⁷ where corrosion rates increased with temperature at different H_2S concentration conditions. The experimental conditions were simulated using the present CO_2/H_2S model, and it was found that the model can predict the change of corrosion rate, as shown in Figure 16.

A corrosion case at more severe conditions was reported by Bich, et al.²⁸ The experimental conditions included high partial pressures of CO_2 ($P_{CO_2} = 3$ bar to 12.8 bar) and H_2S ($P_{H_2S} = 3$ bar to 20 bar). The predicted corrosion rates are within a factor of 2 of the measured data points, as Figure 17 shows.

Long-term flow loop experiments (15 days to 21 days) at high partial pressure of H_2S ($P_{H_2S} = 10$ bar to 30 bar) and high partial pressure of CO_2 ($P_{CO_2} = 3.3$ bar to 10 bar) were conducted by Omar, et al.²⁹ Figure 18 shows a comparison between present electrochemical model prediction and experimental results. The model

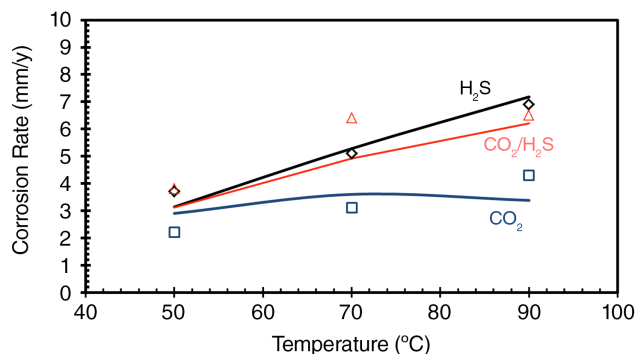


FIGURE 16. Comparison of corrosion rate predictions with experimental results for different temperatures; experimental data shown as points, model predictions shown as lines; total pressure = 1 bar, exposure < 1 h, pH 4.2 (4.5 at 90°C, CO_2), stirring condition. Assumed model parameters: volume ratio for mixture $CO_2/H_2S = 1:1$, flow velocity 0.3 m/s. Data taken from Abayarathna, et al.²⁷

over predicts the corrosion rate by a large factor of 10 to 50. This is due to the formation of iron sulfide layers on the surface, which are not accounted for in the current model. The Sun and Nešić model⁸ considers the effect of iron sulfide corrosion product layers and makes a better prediction for long-term experiments, as Figure 19 shows. Further extension of the current electrochemical model to include mass transfer effects and coverage effect due to iron sulfide layer formation, such as was partly done by Sun and Nešić¹⁰ is ongoing.

CONCLUSIONS

- ❖ A mechanistic study of H_2S corrosion kinetics for X65 steel in short-term exposure was extended to include the effects seen in a mixed H_2S/CO_2 environment.
- ❖ The effect of H_2S on the anodic dissolution of Fe was the same as previously observed behavior in a pure H_2S environment and included retardation or acceleration, depending on the H_2S concentration.
- ❖ An order of magnitude retardation of H_2O reduction due to the presence of H_2S was observed in all experimental conditions; it is postulated that the presence of H_2S also slows down the charge-transfer kinetics of H_2CO_3 reduction by a factor of approximately 3.
- ❖ An electrochemical model of aqueous H_2S corrosion of X65 steel was extended to cover H_2S/CO_2 saturated solutions. The model has been calibrated to fit the new experimental results, and was compared with external data found in the open literature. A good agreement with the experimental data has been obtained for short-term exposures where the effect of iron sulfide corrosion product layers can be ignored.

ACKNOWLEDGMENTS

The authors would like to express sincere appreciation to the following industrial sponsors for

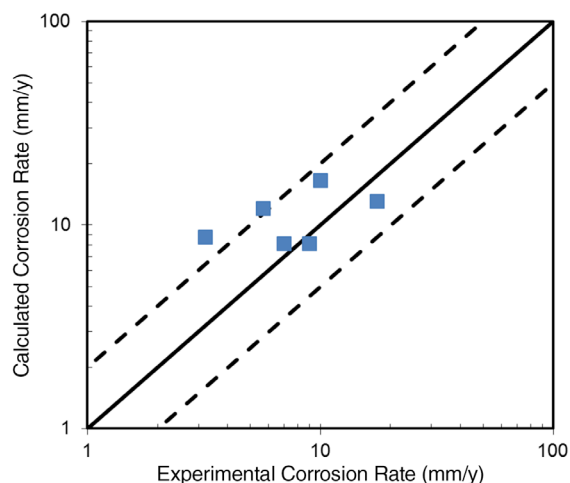


FIGURE 17. Parity plot showing a direct comparison of predicted and experimental corrosion rates; data taken from Bich and Goerz.²⁴ $P_{\text{CO}_2} = 3$ bar to 12.8 bar, $P_{\text{H}_2\text{S}} = 3$ bar to 12.2 bar, pH 5.0, $v = 0.1$ m/s. The solid line represents perfect agreement of experimental and calculated corrosion rates. The dashed lines represent a factor of 2 deviation.

their financial support and direction: BP, Champion Technologies, Chevron, Clariant Oil Services, ConocoPhillips, ENI S. P. A., ExxonMobil, Inpex Corporation, NALCO Energy Services, Occidental Petroleum Co., Petrobras, PETRONAS, PTT, Saudi Aramco, Total, TransCanada, MI-SWACO, HESS and WGIM.

REFERENCES

1. R. Nyborg, "Overview of CO₂ Corrosion Models for Wells and Pipelines," CORROSION/2002, paper no. 02233 (Houston, TX: NACE International, 2002).
2. M.B. Kermani, A. Morshed, *Corrosion* 59 (2003): p. 659-683.
3. S.P. Ewing, *Corrosion* 11 (1955): p. 51-55.
4. J.B. Sardisco, R.E. Pitts, *Corrosion* 21 (1965): p. 245-253.
5. X.L. Cheng, H.Y. Ma, J.P. Zhang, X. Chen, S.H. Chen, H.Q. Yang, *Corrosion* 54 (1998): p. 369-376.
6. M. Singer, B. Brown, A. Camacho, S. Nešić, *Corrosion* 67 (2011): p. 1-16.
7. W. Sun, "Kinetics of Iron Carbonate and Iron Sulfide Scale Formation in Carbon Dioxide/Hydrogen Sulfide Corrosion," Dept. Chem. Eng, Ohio University, 2006.
8. J. Ning, Y. Zheng, D. Young, B. Brown, S. Nešić, *Corrosion* 70 (2014): p. 375-389.
9. A. Anderko, P. McKenzie, R.D. Young, *Corrosion* 57 (2001): p. 202-213.
10. W. Sun, S. Nešić, *Corrosion* 65 (2009): p. 291-307.
11. Y. Zheng, B. Brown, S. Nešić, *Corrosion* 70 (2014): p. 351-365.
12. K. Videm, J. Kvarekval, *Corrosion* 51 (1995): p. 260-269.
13. Y.-S. Choi, S. Nešić, S. Ling, *Electrochimica Acta* 56 (2011): p. 1752-1760.
14. S.N. Smith, J.L. Pacheco, "Prediction of Corrosion in Slightly Sour Environments," CORROSION/2002, paper no. 02241 (Houston, TX: NACE, 2002).
15. E. Abelev, J. Sellberg, T.A. Ramanarayanan, S.L. Bernasek, *J. Mater. Sci.* 44 (2009): p. 6167-6181.
16. S. Nešić, J. Postlethwaite, S. Olsen, *Corrosion* 52 (1996): p. 280-294.
17. D.W. Shoosmith, P. Taylor, M.G. Bailey, D.G. Owen, *J. Electrochem. Soc.* 127 (1980): p. 1007-1015.
18. P. Marcus, E. Protopopoff, *J. Electrochem. Soc.* 137 (1990): p. 2709-2712.
19. S.N. Smith, E.J. Wright, "Prediction of Minimum H₂S Levels Required for Slightly Sour Corrosion," CORROSION/94, paper no. 11 (Houston, TX: NACE, 1994).

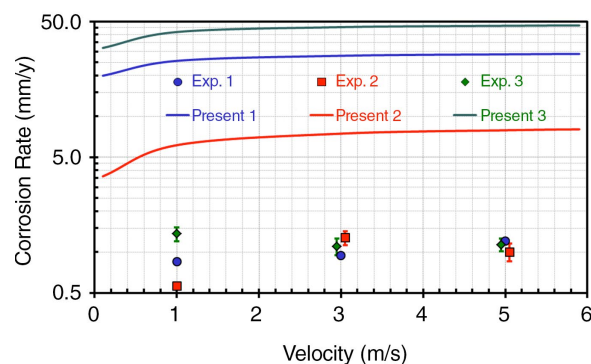


FIGURE 18. Comparison of corrosion rate predictions with experimental results for different velocities; experimental data shown as points, present electrochemical model predictions shown as lines; exp. 1: 19 days, $P_{\text{total}} = 40$ bar, $P_{\text{CO}_2} = 3.3$ bar, $P_{\text{H}_2\text{S}} = 10$ bar, 80°C, pH 3.5, $v = 1$ m/s to 5 m/s; exp. 2: 21 days, $P_{\text{total}} = 40$ bar, $P_{\text{CO}_2} = 3.3$ bar, $P_{\text{H}_2\text{S}} = 10$ bar, 25°C, pH 3.5, $v = 1$ m/s to 5 m/s; exp. 3: 10 days, $P_{\text{total}} = 40$ bar, $P_{\text{CO}_2} = 10$ bar, $P_{\text{H}_2\text{S}} = 30$ bar, 80°C, pH 3.2, $v = 1$ m/s to 5 m/s; experimental data taken from Omar, et al.²⁹

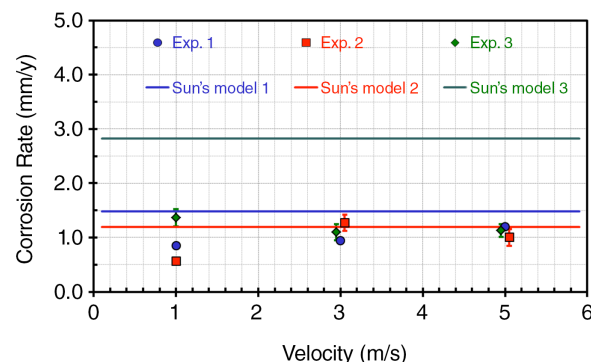


FIGURE 19. Comparison of corrosion rate predictions with experimental results for different velocities; experimental data shown as points, Sun's and Nešić's¹⁰ mass-transfer model predictions shown as lines; Experimental conditions are the same as Figure 18 (reproduced and adapted from Sun and Nešić).¹⁰

20. E. Protopopoff, P. Marcus, *J. Vac. Sci. Technol. Vac. Surf. Films* 5 (1987): p. 944-947.
21. E. Lamy-Pitara, J. Barbier, *J. Electroanal. Chem.* 416 (1996): p. 47-51.
22. J.O. Bockris, D. Drazic, A.R. Despic, *Electrochimica Acta* 4 (1961): p. 325-361.
23. D.E. Jiang, E.A. Carter, *J. Phys. Chem. B* 108 (2004): p. 19140-19145.
24. M. Nordsveen, S. Nešić, N. Nyborg, A. Stangeland, *Corrosion* 59 (2003): p. 433-456.
25. D.A. Palmer, R. Van Eldik, *Chem. Rev.* 83 (1983): p. 651-731.
26. K.L.J. Lee, "A Mechanistic Modeling of CO₂ Corrosion of Mild Steel in the Presence of H₂S" (Ph.D. diss., Ohio University, 2004).
27. D. Abayarathna, A.R. Naraghi, S. Wang, "The Effect of Surface Films on Corrosion of Carbon Steel in a CO₂-H₂S-H₂O System," CORROSION/2005, paper no. 08417 (Houston, TX: NACE, 2005).
28. N.N. Bich, K.G. Goerz, "Caroline Pipeline Failure: Findings on Corrosion Mechanisms in Wet Sour Gas Systems Containing Significant CO₂," CORROSION/96, paper no. 96026 (Houston, TX: NACE, 1996).
29. I.H. Omar, Y.M. Gunaltun, J. Kvarekval, A. Dugstad, "H₂S Corrosion of Carbon Steel Under Simulated Kashagan Field Conditions," CORROSION/2005, paper no. 05300 (Houston, TX: NACE, 2005).